Chipless RFID Tag Exploiting Multifrequency Delta-Phase Quantization Encoding

Simone Genovesi, *Member, IEEE*, Filippo Costa, *Member, IEEE*, Agostino Monorchio, *Fellow, IEEE*, and Giuliano Manara, *Fellow, IEEE*

***Abstract*—A novel encoding paradigm for chipless radio frequency identification (RFID) tags based on phase quantization is presented. The most distinctive features of this approach are represented by the low requirement on bandwidth and by the encoding scheme. The former is achieved by using only a multifrequency reading without resorting to ultrawideband systems, whereas the latter relies on linking the information to the quantized difference between the TE and TM phase response of the tag. The encoding mechanism is described as well as the decoding procedure. The reliability of the illustrated approach is experimentally validated by measurements on fabricated prototypes.**

***Index Terms*—Chipless RFID, differential codification, radio frequency identification (RFID).**

I. Introduction

TRACKING of goods, people localization, remote identification, and access control are only some of the multiple applications in which radio frequency identification (RFID) has been exploited in the recent years [1], [2]. Commercialized RFID tags are mainly passive and consist of an antenna connected to a chip. The probing/interrogating wave coming from the antenna reader induces in the antenna tag an electrical current able to power the integrated circuit, which in turn modulates the backscattered signal collected by the reader. Although the cost of the RFID tags is low, it is desirable to decrease even further for tagging low-price items. To match these needs, chipless RFID tags have been considered as an alternative to the barcode and to the tag equipped with a chip being a good tradeoff in terms of low cost and operational potential [3]–[5]. Chipless RFID is simple to fabricate and does not employ damageable IC, thus it is also suitable to be used in harsh environments or in extreme conditions. The information is still embedded in the electromagnetic response of the tag, but in the absence of a modulating chip, chipless RFID systems generally require an increased reader complexity in order to extract the encoded data. The definition of a unique electromagnetic footprint of each chipless RFID tag has been obtained by exploiting several different approaches. The positioning of deep nulls in the amplitude of the tag frequency response is employed in [5] and [6] for encoding the data. Time-domain techniques are proposed in [8] and [9] to extract the information from the chipless response. The phase response is exploited in [10], whereas cross-polar components are used in [11] and [12]. Hybrid approaches and other paradigms are illustrated in [13]–[15]. This letter illustrates the design of a chipless RFID tag that encodes the information by discretizing the difference (*delta-phase*) between the phase of the reflection coefficient for a TE and a TM plane wave incidence. This solution provides a tag with a reliable coding with respect to the polarization of the incident field. The footprint of the tag can also be considered small if compared to the most part of existing chipless tags. Moreover, the presence of a ground plane in the tag guarantees a configuration less prone to detuning effects due to tagged objects.

A relevant distinctive feature is the small amount of bandwidth required since the encoding mechanism exploits only a few fixed frequencies. The reading can be therefore performed by a multifrequency system without resorting to ultrawideband readers.

This letter is organized as follows. Section II describes the delta-phase quantization encoding strategy, and Section III provides the details for the design. Experimental results are presented in Section IV, whereas conclusions are drawn in Section V.

II. Differential Phase-Encoded Concept

To introduce the delta-phase quantization encoding concept, let us consider the phase response of the periodic surface whose rectangular unit cell is shown in Fig. 1 when illuminated, at normal incidence, both with a TE plane (E-field parallel to x-axis) wave and a TM plane wave (H-field parallel to x-axis). The structure comprises a grounded dielectric substrate with a rectangular loop printed on the top face. A stub of length S is attached in correspondence of each loop corner. The periodicity of the unit cell is equal to $T_x = 1.5$ cm and $T_y = 2$ cm along x- and y-axis, respectively (Fig. 1). The dimension of the rectangular loop is equal to D_x in x-direction and D_y in y-direction.

The unit cell is discretized into a 64×64 pixel matrix for the analysis with a periodic method of moments (PMM) [16]. The width of the rectangular ring and the stub is 1 pixel, as well as the space between the ring side and the stub. Let us fix the dimension $D_x = 58$ pixels and $D_y = 62$ pixels and look at the phase response for two different values of stub length, $S_1 = 12$ pixels and $S_2 = 16$ pixels. The periodic surface is printed on an FR4 dielectric slab ($\varepsilon_r = 4.4 - j0.088$) of thickness $h = 3.6$ mm.

Manuscript received July 17, 2015; accepted August 14, 2015. Date of publication August 20, 2015; date of current version March 16, 2016.

The authors are with the Department of Information Engineering, University of Pisa, 56122 Pisa, Italy (e-mail: simone.genovesi@iet.unipi.it; filippo.costa@iet.unipi.it; a.monorchio@iet.unipi.it; g.manara@iet.unipi.it).

Color versions of one or more of the figures in this letter are available online at http://ieeexplore.ieee.org.

Digital Object Identifier 10.1109/LAWP.2015.2471101

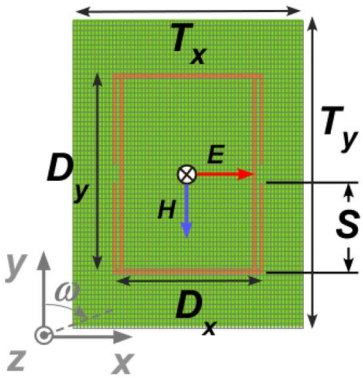

Fig. 1. Top view of the single-loop unit cell of the periodic surface. For a TE plane wave normally impinging on the surface, the electric field E is parallel to x-axis. The 64×64 pixel grid employed by the PMM is shown as well. Angle ω is measured with respect to y-axis.

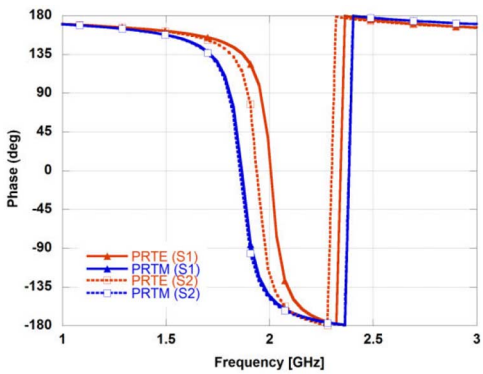

Fig. 2. Phase of the reflection coefficient for both a TE (*PRTE*) and TM (*PRTM*) plane wave incidence impinging on the periodic surface.

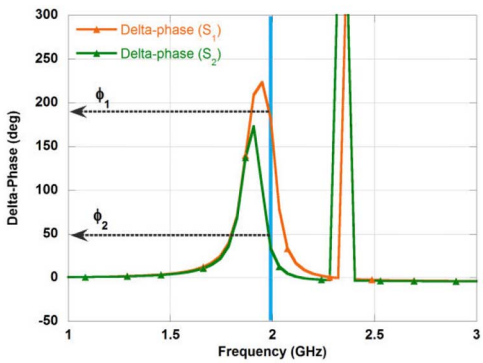

Fig. 3. Delta-phase response for the two stub lengths, S_1 and S_2. Frequency f_1 is highlighted in blue color.

Looking at the phase response in Fig. 2, it can be noticed that even a small change in the stub length leads to an evident shift of the phase response for a TE incident plane wave, whereas the TM response is almost unaffected. The difference between the TE and TM responses is shown in Fig. 3. As highlighted in the plot, it is possible to exploit the delta-phase associated to a particular stub length as a bit codification.

For example, the differential phases exhibited at frequency $f_1 = 2$ GHz for the two stub lengths S_1 and S_2 are ϕ_1 and ϕ_2, and more values can be obtained with different stub lengths. Let us change the stub length and look at the delta-phase value exhibited at frequency f_1. The length is expressed by using the

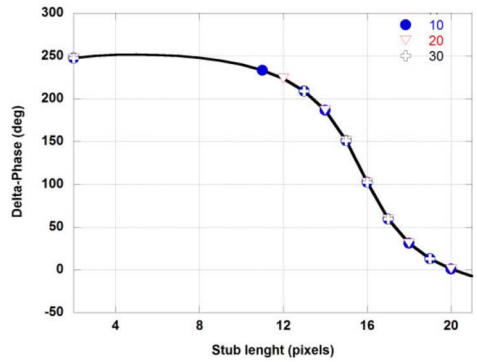

Fig. 4. Quantization of delta-phase at the fixed frequency f_1 for different stub lengths. Pixels are defined as cell periodicity D_y over 64.

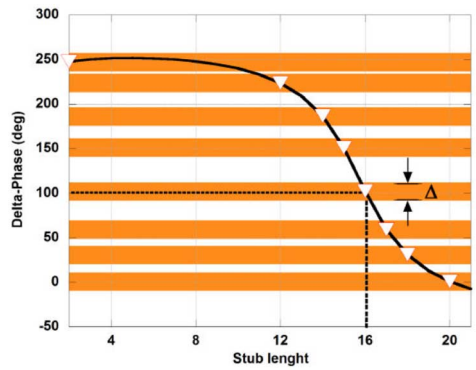

Fig. 5. Decision intervals of the quantized delta-phase defined by a fixed Δ. In this case, a stub length $= 16$ produces a differential phase of $100°$. The information is considered correctly retrieved if the measures delta-phase response is within $[100° - \Delta/2, 100 + \Delta/2]$.

number of pixels composing the stub (Fig. 4). It can be seen that the delta-phase value spans within the interval $(-25°, 250°)$, with short stubs exhibiting the highest differential phase values. Therefore, a stub can encode a multivalue bit with more than two states. The set of stub lengths employed in the codification depends on the criterion used for quantizing and discriminating two phase states. The stubs whose delta-phase differs at least Δ degrees is adopted. It is apparent from Fig. 4 that 10 stub lengths will be available if $\Delta = 10°$, whereas keeping $\Delta = 20°$ or $\Delta = 30°$, the different selectable states will be 8 and 6, respectively. This means that one stubbed ring allows codifying 3 bits if $\Delta = 20°$ is chosen.

The final step is to define the decoding procedure. Let us consider again the delta-phase ϕ at frequency f_1. for $\Delta = 20°$. This choice individuates a set of delta-phases within the interval $[\phi - \Delta/2, \phi + \Delta/2]$, where if $\Delta/2$ is the accepted phase deviation. The individuated intervals do not intersect thus there is no ambiguity in the reading process.

Finally, it is interesting to define the effect of the incident wave angle on the delta-phase behavior. The proposed codification can be employed up to $\omega = 25°$ and $\theta = \pm 30°$.

III. Chipless Tag Design

In order to increase the quantity of information stored in the chipless tag, a structure with four nested rings has been investigated (Fig. 6). Each ring J has its own stubs S^J of equal length attached to the corner and obviously different D_{xJ} and D_{yJ}.

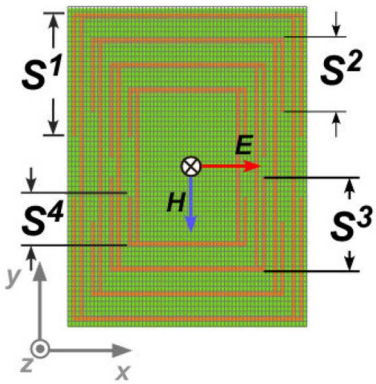

Fig. 6. Top view of the multiloop unit cell of the proposed periodic surface.

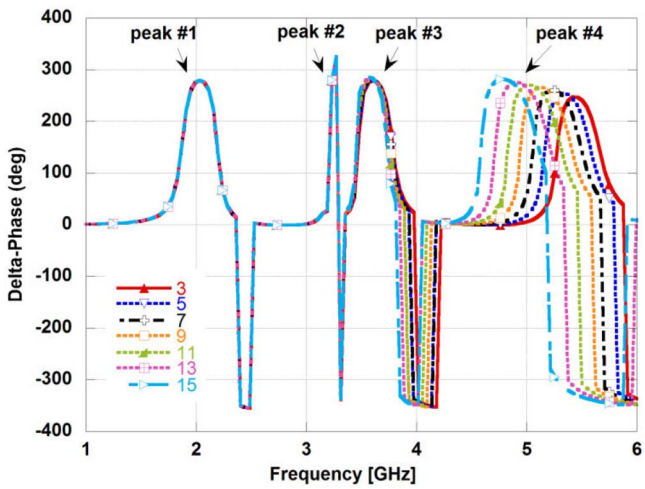

Fig. 7. Variation of the delta-phase response for a structure with the first three stubs fixed ($S^1 = 12$, $S^2 = 8$, and $S^3 = 7$) and the fourth spanning from 3 to 15 pixels.

In this case, the codification of the information is related to the differential phase exhibited by the tag at four fixed frequencies f_i $(i = 1, 2, 3, 4)$.

In order to evaluate the robustness of the employed unit-cell configuration, it is important to verify that the differential phase response of one ring is not altered by the change in the stub lengths of the other elements. Let us consider, for example, a critical case when the first three stubs are fixed with intermediate lengths ($S^1 = 12$, $S^2 = 8$, and $S^3 = 7$) and the fourth spanning from 3 to 15 pixels. It can be seen that the delta-phase curve is changing only in correspondence of the peak #4, the one associated to the fourth ring.

Therefore, the change in the delta-phase exhibited at the frequencies f_i is mostly related to the stub length of the corresponding ring, and it is weakly related to the adjacent elements. The behavior is confirmed when the current distribution on the unit cell at the four design frequencies is observed (Fig. 8). The frequencies f_i and the relevant pixel lengths for describing the structure are summarized in Table I.

Let us now calculate the number of states encoded by the described structure. Considering $\Delta = 10°$, the total number of combinations is equal to 13 104, that is 13.67 bits, whereas by choosing $\Delta = 30°$ the bit number is 10.49. Contrarily to many

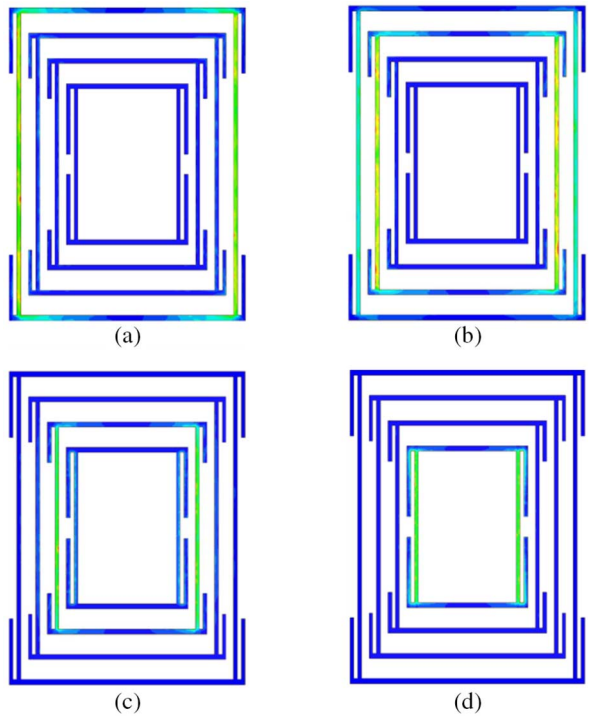

Fig. 8. Normalized current distribution at the resonance of (a) element#1 at f_1, (b) element#2 at f_2, (c) element#3 at f_3, and (d) element#4 at f_4.

TABLE I
PIXEL DIMENSION OF EACH RING AND CONNECTED STUB

Element#1	Element#2	Element#3	Element#4
$D_{x1} = 58$	$D_{x2} = 48$	$D_{x3} = 38$	$D_{x4} = 28$
$D_{y1} = 62$	$D_{y2} = 52$	$D_{y3} = 42$	$D_{y4} = 32$
$S^1 = 12$	$S^2 = 8$	$S^3 = 7$	$S^4 = 13$
$f_1 = 2$ GHz	$f_2 = 2.86$ GHz	$f_3 = 3.82$ GHz	$f_4 = 4.93$ GHz

TABLE II
QUANTIZED DELTA-PHASE VALUES OBTAINED FOR DIFFERENT Δ FOR A CHIPLESS RFID REALIZED ON THE FR4 SUBSTRATE

	Δ=10°	**Δ =20°**	**Δ =30°**
Element#1	13	10	8
Element#2	9	5	4
Element#3	14	12	9
Element#4	8	6	5
combinations	13104	3600	1440
bits	13.67	11.81	10.49
bits/Band.	3.41	2.95	2.62

encoding schemes that require an ultrawide or wideband occupation, the proposed codification paradigm requires the chipless RFID tag phase response at four fixed frequencies only. Therefore, the number of bits per megahertz allocated at a single frequency spans from 3.41 to 2.62, for $\Delta = 10°$ and $\Delta = 30°$, respectively (Table II).

Finally, it is remarked that a substrate with a lower dielectric permittivity, such as Teflon ($\varepsilon_r = 2.17 - j0.0022$) could guarantee a less steep phase response, and therefore more discrete-phase states are available. By considering the same unit cell size (T_x, T_y), more combinations are obtained (Table III) although the f_i frequencies are obviously shifted at higher values

TABLE III
QUANTIZED DELTA-PHASE VALUES OBTAINED FOR DIFFERENT Δ FOR A CHIPLESS RFID REALIZED ON THE TEFLON SUBSTRATE

	Δ=10°	Δ =20°	Δ =30°
Element#1	18	11	9
Element#2	15	12	11
Element#3	12	11	8
Element#4	8	6	5
combinations	25920	8712	3960
bits	14.66	13	11.95
bits/Band.	3.67	3.25	2.99

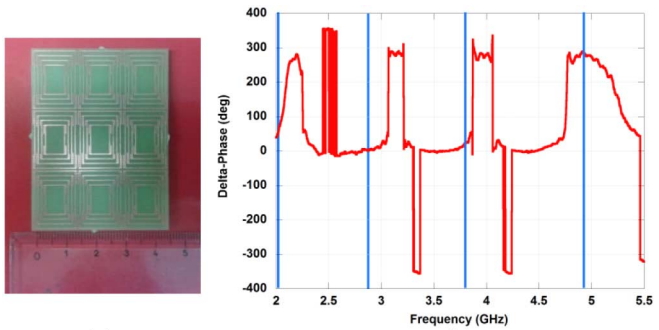

(a) (b)

Fig. 9. (a) Prototype of the chipless RFID tag comprising 3 × 3 unit cells and (b) quantized phase encoding (frequencies f_i are highlighted in blue).

($f_1 = 2.8$ GHz, $f_2 = 4$ GHz, $f_3 = 5.1$ GHz, $f_4 = 6.5$ GHz). In particular, the number of combinations is almost doubled for $\Delta = 10$ and almost tripled for $\Delta = 30$.

IV. EXPERIMENTAL RESULTS

Several chipless RFID tags have been fabricated and measured to assess the performance of the proposed quantized delta-phase encoding scheme. A finite-size tag comprising 3×3 unit cells has been reported in Fig. 9(a) as a representative example. The tag has been placed at 50 cm in front of two dual-polarized wideband horn antennas (Flann DP280). An Agilent E5071 C vector network analyzer has been employed for collecting the scattering parameters in a nonanechoic environment [6]. Fig. 9(b) reports a measured frequency response with the occupied frequency band highlighted with blue vertical bars. It is important to highlight that only these frequencies are employed in the reading process since the delta-phase encoding needs only a few fixed frequencies. Therefore, the reader is based on a multifrequency narrowband probe avoiding wideband or ultrawideband radiators.

Indeed, the more cells employed, the higher the physical footprint of the tag, and thus the radar cross section. By using a 3×3-unit-cells tag, we have obtained a read range of 50 cm with an input power of 0 dBm. A longer read range could be achieved by using more unit cells (*i.e.*, 4×4 or 5×5) for each tag [6]. The comparison between simulation and measurements for the chipless RFID tag comprising 3×3 unit cells is provided in Table IV. Similar performance has been observed in all the manufactured tags and suggests that a $\Delta = 20°$ can be considered a good choice able to guarantee the tradeoff between encoding capacity and correct recovering of the information.

TABLE IV
COMPARISON BETWEEN SIMULATIONS AND MEASUREMENTS

Element#	Stub length (pixel)	Simulated delta phase (deg)	Measured delta phase (deg)	Error (deg)
1	15	22	30	8
2	12	6	3.5	2.5
3	10	7	16	9
4	13	275	284	9

V. CONCLUSION

A new chipless RFID tag based on a quantized delta-phase encoding has been illustrated. The information is encoded in the quantized values of the difference between the TE and TM phase responses. This encoding paradigm has low requirement on bandwidth, and it can be implemented by a multifrequency reader without resorting to ultrawideband systems. The performance has been assessed by measurements on fabricated prototypes.

REFERENCES

[1] K. Finkenzeller, *RFID Handbook: Radio-frequency Identification Fundamentals and Applications*. New York, NY, USA: Wiley, 2004.
[2] C. Occhiuzzi, S. Caizzone, and G. Marrocco, "Passive UHF RFID antennas for sensing applications: Principles, methods, and classifications," *IEEE Antennas Propag. Mag.*, vol. 55, no. 6, pp. 14–34, Dec. 2013.
[3] R. R. Fletcher, "Low-cost electromagnetic tagging: design and implementation," Ph.D. dissertation, Massachusetts Institute of Technology, Cambridge, MA, USA, 2002.
[4] S. Tedjini *et al.*, "Hold the chips: Chipless technology, an alternative technique for RFID," *IEEE Microw. Mag.*, vol. 14, no. 5, pp. 56–65, Jul. 2013.
[5] S. Preradovic and N. C. Karmakar, "Chipless RFID: Bar code of the future," *IEEE Microw. Mag.*, vol. 11, no. 7, pp. 87–97, Dec. 2010.
[6] F. Costa, S. Genovesi, and A. Monorchio, "A chipless RFID based on multiresonant high-impedance surfaces," *IEEE Trans. Microw. Theory Tech.*, vol. 61, no. 1, pp. 146–153, Jan. 2013.
[7] S. Preradovic, I. Balbin, N. C. Karmakar, and G. F. Swiegers, "Multiresonator-based chipless RFID system for low-cost item tracking," *IEEE Trans. Microw. Theory Tech.*, vol. 57, no. 5, pp. 1411–1419, May 2009.
[8] A. T. Blischak and M. Manteghi, "Embedded singularity chipless RFID tags," *IEEE Trans. Antennas Propag.*, vol. 59, no. 11, pp. 3961–3968, Nov. 2011.
[9] A. Ramos, A. Lazaro, D. Girbau, and R. Villarino, "Time-domain measurement of time-coded UWB chipless RFID tags," *Prog. Electromagn. Res.*, vol. 116, pp. 313–331, 2011.
[10] I. Balbin and N. C. Karmakar, "Phase-encoded chipless RFID transponder for large-scale low-cost applications," *IEEE Microw. Wireless Compon. Lett.*, vol. 19, no. 8, pp. 509–511, Aug. 2009.
[11] F. Costa, S. Genovesi, and A. Monorchio, "Chipless RFIDs for metallic objects by using cross polarization encoding," *IEEE Trans. Antennas Propag.*, vol. 62, no. 8, pp. 4402–4407, Aug. 2014.
[12] A. Vena, E. Perret, and S. Tedjni, "A depolarizing chipless RFID tag for robust detection and its FCC compliant UWB reading system," *IEEE Trans. Microw. Theory Tech.*, vol. 61, no. 8, pp. 2982–2994, Aug. 2013.
[13] A. Vena, E. Perret, and S. Tedjini, "Chipless RFID tag using hybrid coding technique," *IEEE Trans. Microw. Theory Tech.*, vol. 59, no. 12, pp. 3356–3364, Dec. 2011.
[14] A. Lazaro, A. Ramos, D. Girbau, and R. Villarino, "Chipless UWB RFID tag detection using continuous wavelet transform," *IEEE Antennas Wireless Propag. Lett.*, vol. 10, pp. 520–523, 2011.
[15] C. Mandel, B. Kubina, M. Schüßler, and R. Jakoby, "Metamaterial-inspired passive chipless radio-frequency identification and wireless sensing," *Ann. Telecommun.*, vol. 68, no. 7–8, pp. 385–399, Aug. 2013.
[16] R. Mittra, C. H. Chan, and T. Cwik, "Techniques for analyzing frequency selective surfaces—A review," *Proc. IEEE*, vol. 76, no. 12, pp. 1593–1615, Dec. 1988.